Transmission of low energy (16O+ ions through condensed ammonia and water overlayers

Mustafa Akbulut, Norbert J. Sack, and Theodore E. Madey

Citation: The Journal of Chemical Physics **103**, 2202 (1995); doi: 10.1063/1.469695
View online: http://dx.doi.org/10.1063/1.469695
View Table of Contents: http://scitation.aip.org/content/aip/journal/jcp/103/6?ver=pdfcov
Published by the AIP Publishing

Transmission of low energy (<10 eV) $^{16}O^+$ ions through condensed ammonia and water overlayers

Mustafa Akbulut,[a] Norbert J. Sack,[b] and Theodore E. Madey[c]
Rutgers, The State University of New Jersey, Department of Physics and Astronomy and Laboratory for Surface Modification, Piscataway, New Jersey 08855

(Received 24 January 1995; accepted 3 May 1995)

We have studied the transmission of low energy (<10 eV) $^{16}O^+$ ions through ultrathin films of condensed molecular solids, NH_3 and $H_2{}^{18}O$, in order to address the fundamental scattering processes that occur in the desorption of ions from below the surface of solids. $^{16}O^+$ ions with a peak energy of ~7 eV and a narrow angular distribution [full-width at half-maximum (FWHM) ~15°] are generated by means of electron stimulated desorption (ESD) from an ^{16}O oxidized W(100) surface and their yield, energy and angular distribution are measured with a digital ESDIAD (ESD ion angular distribution) detector. Ultrathin NH_3 and $H_2{}^{18}O$ films of known thickness are condensed on the oxidized surface at 25 K and changes in the ion yield, energy and angular distribution are observed as a function of coverage. We find that adsorption of only 0.5 monolayer of $H_2{}^{18}O$ is enough to suppress the $^{16}O^+$ ion emission by a factor of 100, while three monolayers of NH_3 are necessary for equivalent suppression of the $^{16}O^+$ ion emission. The angular distribution of the ions increases slightly with increasing overlayer coverage. We also find that a small percentage of $H_2{}^{18}O$ dissociates upon adsorption. We suggest that one electron charge transfer between $^{16}O^+$ and $H_2{}^{18}O$, and between $^{16}O^+$ and the dissociation product OH are the main reasons for the strong attenuation of $^{16}O^+$ ions by only a fraction of a monolayer of $H_2{}^{18}O$. Charge transfer is also believed to be the main process that causes suppression of $^{16}O^+$ ions by ultrathin NH_3 films. Other elastic and inelastic processes are not believed to contribute significantly to $^{16}O^+$ attenuation in NH_3 or $H_2{}^{18}O$ films. © *1995 American Institute of Physics.*

I. INTRODUCTION

Electronic excitation of surface species by means of electrons, photons, or ions can lead to the desorption both of neutrals (including metastables) and ions.[1,2] Electrons and photons with energies in the range 15–1000 eV can penetrate a solid and cause electronic excitations below the surface if their energy is greater than the excitation threshold energy. A fundamental issue in desorption induced by electronic transition (DIET) processes is the depth of origin of the desorption species.[3–5] An understanding of the depth of origin is important since it permits elucidation of the processes which govern ion desorption in DIET.

It is generally assumed for DIET processes that the ion neutralization probability near a surface is large enough to prevent ion emission except from the top atomic layer. This assumption is valid for DIET from an adsorbed molecular monolayer on a metal surface, where all desorbing species originate from the adsorbed monolayer.[1] However, for compound materials such as oxides, it is possible that a few surface layers may contribute to the desorption yield in DIET.[3,6] Recently, we have found that low energy ions (<10 eV) created below a surface can penetrate a rare gas film 4 or 5 atomic layers thick.[7–9]

The elastic and inelastic processes (such as energy transfer and charge transfer) that occur in the DIET of low energy ions from the surfaces of solids depend on the nature of the ion and its kinetic energy, and on the structure and electronic properties of the surface materials. However, the processes and properties that determine the depth of origin of desorbing species that originate from the layers beneath the surface are not yet understood in detail.

Moreover, in electrochemistry and interface science, ion and electron transport through surface layers is of fundamental interest. Electrode processes, i.e., heterogeneous chemical reactions taking place at the electrode–electrolyte interface, involve the interfacial movement of electrons and ions associated with charge transfer across the interface. Irrespective of the source of ions, in all ion transport processes through specific ultrathin overlayer films, the main physical mechanisms of scattering and charge transfer should be basically the same. Hence, the investigations of ion transport processes through surface layers of H_2O can be relevant to the understanding of heterogeneous electrochemical processes as well.

Charge transfer is the dominant *inelastic* process in determining the desorption probability of atomic ions from a surface.[10–12] During electron stimulated desorption (ESD) of a positive ion from a conducting surface, the energy levels of the ion broaden and shift, and the ion may undergo charge transfer by resonant tunneling from the occupied levels of the substrate [resonant neutralization (RN)] or by Auger-type processes involving two electrons [Auger neutralization (AN)]. Auger neutralization arises from coupling between the discrete energy levels of the ion and the continuum electronic states of the substrate.[13] Negative ions can be formed or neutralized by resonant tunneling during desorption.[14] The desorption of positive and negative ions may also be

[a]Permanent address: Stevens Institute of Technology, Department of Physics, Hoboken, New Jersey 07030.
[b]Present address: McKinsey & Co., Inc., Kurfürstendamm 185, D-10707 Berlin, Germany.
[c]Author to whom correspondence should be addressed.

 0021-9606/95/103(6)/2202/14/$6.00

affected by the presence of coadsorbed species or neighboring adsorbates;[15,16] charge and energy transfer between the desorbing ion and its neighboring molecules have been found to influence the ion desorption rate.[17] A major challenge is to distinguish the influence of ion–substrate interactions from ion–overlayer interactions on the ion desorption probability.[7,18]

In order to determine elastic and inelastic processes that influence ion desorption through overlayer films, we are systematically studying the interaction of various low energy ions with a variety of overlayers having different electronic and chemical properties. Using a novel experimental approach we attempt to distinguish ion–substrate interactions from ion–overlayer interactions by viewing a substrate as a source of ions created by electronic excitations.[7] We have reported our first results on the transmission of ESD produced positive oxygen ions through ultrathin films of Ar, Kr, and Xe, and we have demonstrated that some oxygen ions can penetrate several monolayers of rare gas films.[7–9]

In the present study, we report on the transmission of $^{16}O^+$ ions generated by means of ESD from an oxidized W(100) surface through condensed molecular overlayers of NH_3 and $H_2{}^{18}O$. In a first experiment on transmission of O^+ through NH_3 on a crystalline TiO_2(110) substrate, evidence was found for a charge transfer mechanism.[18] The goal of the present experiment is to explore the substrate dependence of ion transmission through ultrathin molecular films and to develop a better understanding of how overlayer electronic and chemical properties affect the ion transmission. We have chosen NH_3 and $H_2{}^{18}O$ as overlayers for several reasons. First, their electronic interaction with the oxidized W(100) surface is expected to be sufficiently weak that the initial electronic excitation leading to the desorption of O^+ ions from the substrate may not be affected substantially by the presence of the overlayers. Second, their close masses and isoelectronic structure, but their different ionization energies (in gas phase, ~10.17 eV for NH_3 and ~12.61 eV for H_2O), will allow us to distinguish elastic collisions from charge transfer collisions, which occur during $^{16}O^+$ passage through NH_3 and $H_2{}^{18}O$. Third, the ion–molecule interaction, especially the ion–water interaction, is of fundamental interest in electrochemistry. Finally, this experiment involving adsorbed NH_3 and $H_2{}^{18}O$ layers provides new information about the adsorption and reaction of NH_3 and $H_2{}^{18}O$ on an oxidized surface. In this paper, we focus on the $^{16}O^+$ ion transmission through NH_3 and $H_2{}^{18}O$. The details of the surface chemistry of $H_2{}^{18}O$ on the oxidized W(100) are not presented here, but are discussed extensively in a forthcoming paper.[19] As needed for the present discussion, some conclusions about the surface chemistry of $H_2{}^{18}O$ on the oxidized W(100) are given.

In Sec. II we describe the experimental techniques and the sample preparation. Section III begins with the surface chemistry of NH_3 and $H_2{}^{18}O$ on the oxidized W(100) surface and finishes with the presentation of the oxygen ion transmission through $H_2{}^{18}O$ and NH_3 overlayer films. Thermal desorption spectroscopy (TDS) and ESD are used to determine the coverage of $H_2{}^{18}O$ and NH_3 on the oxidized W(100) surface and to study the surface chemistry of $H_2{}^{18}O$ and NH_3. In Sec. IV, we present a discussion of the experimental results and an attenuation model for the O^+ transmission through ultrathin films of NH_3 and $H_2{}^{18}O$. Conclusions are given in Sec. V.

II. EXPERIMENTAL SETUP

The experiments are performed in an ultrahigh vacuum (UHV) chamber equipped with facilities for surface characterization including thermal desorption spectroscopy (TDS), low energy electron diffraction (LEED), low energy ion scattering (LEIS), Auger electron spectroscopy (AES), and electron stimulated desorption ion angular distribution (ESDIAD); details of the apparatus and the methods used have been described previously.[8]

The sample, a W(100) crystal, is mounted on a manipulator on which it can be cooled to ~25 K by means of a closed cycle He refrigerator. The sample can be heated in the range of 25–1600 K by radiative heating and electron beam heating from a tungsten filament. The temperature is measured by using a Ni/Cr/Si–Ni/Si/Mg, *N*-type (generally known as Nicrosil–Nisil), thermocouple.

In order to form an ultrathin oxide film the crystal is heated in oxygen (5×10^{-6} Pa) for 10 min at 860 K. The oxidized surface prepared in this way exhibits a (1×3) LEED pattern, and ESD of this surface produces a well defined $^{16}O^+$ beam having a peak energy of ~7 eV and full-width at half-maximum (FWHM) of ~15° desorbing normal to the surface. AES spectra from the oxidized surface indicate that the surface is essentially clean with a very small carbon impurity (0.05 ML). Based on earlier studies,[20,21] the stoichiometry of the surface is assumed to be about $WO_{2\text{-}3}$.

Since we study the transmission of O^+ ions through the water overlayer which contains oxygen, the W(100) surface is oxidized with ^{16}O, and water containing the oxygen isotope ^{18}O ($H_2{}^{18}O$) is used in order to distinguish the ESD ions desorbing from the oxidized W(100) surface from the adsorbed water layers. Use of isotopically labeled water also allows us to study the reaction of water with the oxide substrate. Using a quadrupole mass spectrometer (QMS) as an ESD detector (QMS/ESD detector), $^{16}O^+$ and $^{18}O^+$ can be well resolved.

The overlayer gases, NH_3 and $H_2{}^{18}O$ are purified in several freeze–pump–thaw cycles. They are dosed onto the sample surface via separate leak valves through two directional beam dosers capped with microcapillary arrays aimed at the surface. This procedure permits precise dosing of various coverages of the gas from fractional monolayer to multilayers. The exposure in units of langmuir (L) is determined by measuring the dosing pressure with an uncalibrated ionization gauge, and the dosing time. However, note that because the doser produces a broad molecular beam onto the sample, the flux onto the surface is greater than the random background flux detected using the ionization gauge. Since the dosers are positioned differently with respect to the sample and the dosing geometry is very important parameter for determining the molecular flux on a surface for a direct dosing, we expect differences between NH_3 and $H_2{}^{18}O$ exposures corresponding to monolayer coverages of NH_3 and $H_2{}^{18}O$ determined in units of langmuir.

The coverage of the molecular overlayers is determined using thermal desorption spectroscopy (TDS), which allows us to resolve the desorption peaks from the first monolayer and subsequent multilayers.

Positive oxygen ions are generated by bombarding the clean oxidized W(100) surface with a focused 300 eV electron beam. The ions are detected by means of a high sensitivity digital ESDIAD/TOF (time-of-flight) detector that allows mass, energy, and angle resolved ion detection. It includes a set of four high transparency planar grids of which all except the second are grounded, a stack of five microchannel plates, and a position sensitive resistive anode encoder (RAE). The RAE is connected to a position analyzing computer to provide direct digital acquisition of two-dimensional data. By pulsing the primary electron beam, which provides a start pulse coincident with desorption from the surface, and by gating the retarding potential grid G_2, we can perform TOF analysis of the desorbing ions. The TOF capability allows us to separate easily lighter ions (shorter flight times) from heavier ions (longer flight times). For example, using the ESDIAD/TOF detector, we can separate easily H^+, O^+, and CO^+ signals from each other. However, note that using the ESDIAD/TOF detector, we cannot resolve ions with similar masses such as $^{16}O^+$ and $^{18}O^+$. For appropriate bias and pulse conditions we can detect ions in a velocity resolved mode. Typically, the electron pulse length is 0.1 μs, the average electron current is 1 nA, and the total electron fluence for a measurement is $\sim 2\times 10^{13}$ cm^{-2} (beam area ~ 1 mm^2).

The polar angle of detection (under field free conditions around the crystal) ranges from 0° to 22°. Application of a positive bias voltage to the substrate compresses the angular distribution of the desorbing positive ions so that even ions which desorb with angles substantially larger than 22° can be detected. When a substrate bias of +100 V is applied, the polar angle of detection is increased from 0° to 22° to 0° to 70° for a positive ion with a kinetic energy ~7 eV. Hence, the application of a positive sample bias allows us to collect nearly the total O^+ desorption yield, but it makes the quantitative measurement of the angular and energy distribution of desorbing ions more difficult. In this work, the angle integrated O^+ desorption yields are determined both under field free conditions (zero sample bias) and with a substrate bias of +100 V, while the ion angular and energy distributions are determined under field free conditions. Hereafter, the ion detection under zero sample bias is referred to as ''small angle of detection,'' and the ion detection with a substrate bias of +100 V is referred to as ''large angle of detection.''

We can also detect the ESD ions with a QMS detector with its ionizer filament turned off. The QMS as an ESD detector is used to resolve the ions that are close in mass such as $^{16}O^+$, $^{18}O^+$, $^{16}OH^+$, and $^{18}OH^+$. The QMS detector enables us to measure angle resolved ion yields (acceptance angle ~4°) with high mass resolution and to confirm the ESDIAD normalized ion yields as a function of coverage.

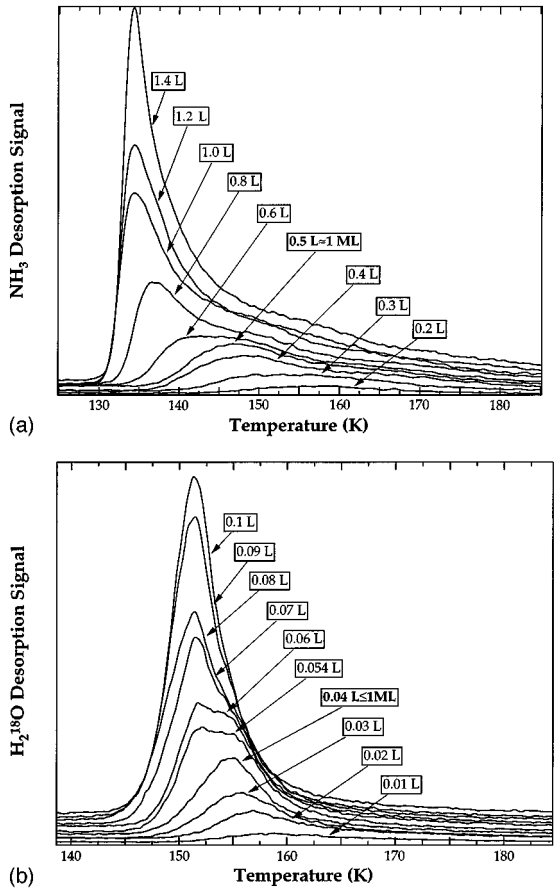

FIG. 1. TDS spectra after adsorption of various exposures of (a) NH_3 and (b) $H_2{}^{18}O$ on oxidized W(100) surface at 25 K.

III. RESULTS

A. Determination of overlayer coverage

In order to determine the coverage of NH_3 and $H_2{}^{18}O$ on the oxidized W(100) surface, we perform TDS and LEIS experiments. Since the first monolayer and subsequent multilayer desorption peaks are identified in TDS, the relation between coverage and exposure can be determined and calibrated.

Figures 1(a) and 1(b) show a series of thermal desorption spectra from NH_3 and $H_2{}^{18}O$ adsorbed on the oxidized W(100) at 25 K, respectively. At low exposure (<0.50 L for NH_3 and <0.04 L for $H_2{}^{18}O$), there is only a single desorption peak for NH_3 and $H_2{}^{18}O$. The lower the exposure, the higher the desorption temperature. With increasing exposure the desorption peak temperatures shift to lower temperatures and the desorption peaks at ~148 K for NH_3 and ~155 K for $H_2{}^{18}O$ stop growing in intensity above exposures of ~0.5 L and ~0.04 L, respectively, where a second low temperature peak is observed to form in each case. For calibration, we define that the coverages (and exposures) corresponding to saturation of the 148 K peak (for NH_3) and 155 K peak (for $H_2{}^{18}O$) correspond to monolayer coverages. Note that the ML exposures differ significantly for NH_3 and $H_2{}^{18}O$ on the oxidized W(100) surface. We believe that this difference is mainly due to our use of two separate molecular beam dos-

ers, to different dosing geometry, to the uncalibrated ion gauge and to different wall pumping effects.

In each case, the second peak starts growing after completion of the monolayer peak, and continues to increase with increasing exposure without saturating. At high coverages, the spectra have a common leading edge, consistent with zeroth-order desorption. Ice sublimation is a zeroth-order process, which requires that the rate of desorption at any given temperature is independent of coverage. Zeroth-order desorption kinetics also require that the peak temperature increases with increasing coverage, as the thick layers are depleted. Therefore, based on our observations, we assign the second peaks as due to desorption from multilayers.

In order to confirm the TDS coverage calibration for $H_2{}^{18}O$, we perform LEIS experiments. As discussed in detail in the forthcoming paper,[19] we conclude that within experimental uncertainty, the LEIS result is consistent with the TDS monolayer calibration (1 ML corresponds to 0.04 L).

Based on the results of earlier investigations,[20–23] we assume that the stoichiometry of the oxidized W(100) surface is approximately $WO_{2\text{-}3}$. We can use the unit cell of WO_2 which has dimensions of $\sim$4.86 Å$\times$4.86 Å,[24] to define the overlayer coverages. Considering the intermolecular interactions, such as dipole–dipole interactions between NH_3–NH_3 or $H_2{}^{18}O$–$H_2{}^{18}O$ molecules, and the van der Waals diameter of overlayer molecules (3.6 Å for NH_3 and 2.9 Å for $H_2{}^{18}O$),[25,26] we can define that one monolayer (ML) of NH_3 corresponds to one NH_3 per unit cell or 4.25×10^{14} molecules/cm^2 and one ML of $H_2{}^{18}O$ corresponds to two $H_2{}^{18}O$ molecules per unit cell or 8.5×10^{14} molecules/cm^2 on the oxidized W(100) surface. These coverages for NH_3 and $H_2{}^{18}O$ on oxidized W(100) are very close to the monolayer coverages of water and ammonia reported for other metal and oxide surfaces.[25,27–29] For example, a bilayer of water on the Ru(0001) surface[28,30] has a coverage of $\sim1\times10^{15}$ molecules/cm^2, which is very close to the above estimated coverage of $H_2{}^{18}O$ on the oxidized W(100) surface. The uncertainty in our monolayer coverage identification is estimated to be $\pm$20%.

B. Adsorption kinetics and reaction of overlayer molecules

The integral of a TDS peak over time is proportional to the total number of particles which desorb. Figure 2 shows the area integrated NH_3 TDS intensity as a function of NH_3 exposure. Both NH_3 and $H_2{}^{18}O$ TDS intensities increase linearly with exposure above about 0.1 L for NH_3 (Fig. 2) and about 0.0032 L for $H_2{}^{18}O$ (Ref. 19). The linearity of these curves indicates that the sticking probabilities for both NH_3 and $H_2{}^{18}O$ are constant. No NH_3 and $H_2{}^{18}O$ TDS signals are detected for exposures below $\sim$0.1 L for NH_3 and $\sim$0.0032 L for $H_2{}^{18}O$. These offsets in the area-integrated TDS intensities show that the first molecules that adsorb do not desorb molecularly; we suggest that they dissociate. Assuming that the sticking probabilities do not change, we can derive that $\sim$0.2 ML of NH_3 and $\sim$0.08 ML of $H_2{}^{18}O$ dissociate. However, from these results alone, it is not clear if dissociation occurs upon adsorption or during desorption.

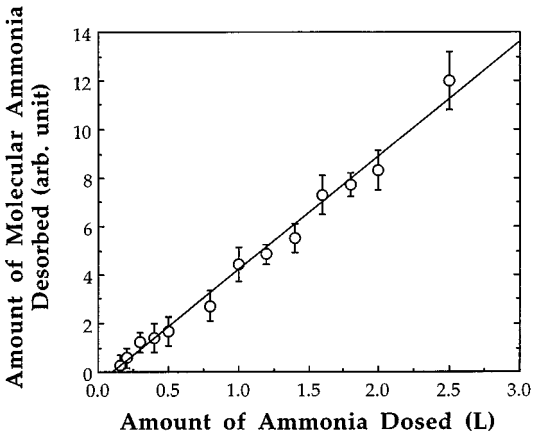

FIG. 2. TDS integrated area as a function of NH_3 exposure.

In order to investigate further the adsorption of the overlayer molecules on the oxidized surface, we carry out ESD experiments using the QMS as an ESD detector (ESD/QMS detector). After adsorption of a fraction of a monolayer of $H_2{}^{18}O$ on the oxidized W(100) surface, ESD measurements made using the ESD/QMS detector indicate the presence of H^+, $(^{16}OH)^+$ and $(^{18}OH)^+$ signals, in addition to O^+ signals. As discussed in more detail in the forthcoming paper,[19] the observation of ESD $(^{16}OH)^+$ and $(^{18}OH)^+$ signals implies that a small percentage of a monolayer of $H_2{}^{18}O$ dissociates upon adsorption.

In order to determine the stability of molecularly adsorbed $H_2{}^{18}O$ and its dissociation products (OH species) on the oxidized W(100) surface, the influence of crystal heating on the ESD signals is investigated. As discussed in the forthcoming paper,[19] no stable $H_2{}^{18}O$ and OH species remain on the oxidized W(100) surface above $\sim$350 K; OH desorbs by heating at around 260–350 K.

In order to obtain the clean oxidized W(100) surface after adsorption of $H_2{}^{18}O$ on the surface, the sample is annealed at $\sim$600 K. Following annealing the sample at $\sim$600 K, the ESD measurement made with the QMS/ESD detector at 25 K demonstrates a relatively large $^{16}O^+$ and small $^{18}O^+$ signal. Both $^{16}O^+$ and small $^{18}O^+$ originate from the oxide state. Decomposition of $H_2{}^{18}O$ to form adsorbed surface species (OH) and further reaction of the adsorbed species at higher temperature results in adsorbed ^{18}O atoms on the surface. The adsorbed ^{18}O atoms convert from an adsorbed state to an oxide state when the sample is annealed between 300 K and 600 K. We discuss the formation of surface ^{18}O and oxidation of the surface with ^{18}O in more detail in the forthcoming paper.[19]

ESD of NH_3 on the oxidized W(100) produces only H^+ ions from the adsorbate and $^{16}O^+$ ions from the substrate. The influence of crystal heating on ESD is studied; no $(OH)^+$ signal is detected from NH_3 adsorbed on the oxidized W(100) surface at any temperature within the detectibility limits. The level of detectibility of $(OH)^+$ is estimated to be $\sim$1% of H^+. This indicates either that no OH species are formed or that dissociation leads to formation of lattice OH species that do not produce an ESD $(OH)^+$ signal. [Note that we distinguish between adsorbed OH (which correspond to

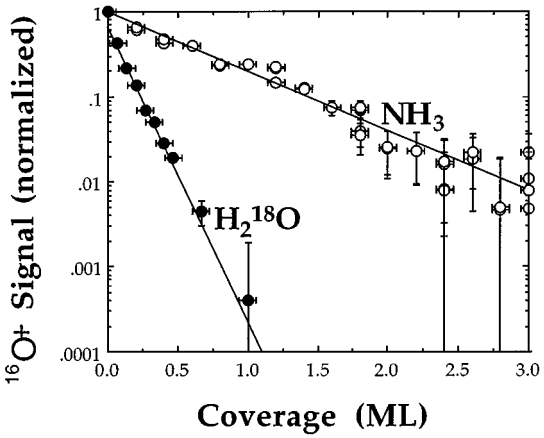

FIG. 3. Total angle integrated $^{16}O^+$ yield as a function of NH_3 (close circles) and $H_2{}^{18}O$ (open circles) coverage on a semilogarithmic plot (sample bias, 100 V). The data are normalized to 1 for the clean surface value.

OH fragments from $H_2{}^{18}O$ dissociation, bonded to a surface cation site) and lattice OH. A lattice OH, $(OH)^{\delta-}$, can be formed when an atomic hydrogen ion bonds to a lattice oxygen ion.] Following each TDS measurement (25 K$\leqslant T\leqslant$270 K) from NH_3 adsorbed on the oxidized W(100) surface,
the original $^{16}O^+$ signal from the clean surface is reestablished and the H^+ signal disappears. If any adsorbates were to remain on the surface after the TDS measurements, the original $^{16}O^+$ signal could not be re-established due to elastic and inelastic processes between the desorbing $^{16}O^+$ ions and the dissociation fragments following the annealing measurements.[19] Since the only condition to re-establish the original ESD $^{16}O^+$ signal is to obtain the clean oxidized W(100) surface, our observations suggest that no dissociation products remain on the surface above 270 K.

C. Oxygen ion desorption through NH_3 and $H_2{}^{18}O$ layers

Using a focused 300 eV electron beam, ESD $^{16}O^+$ ions are generated from the oxidized surface at 25 K and their yield, energy and angular distributions are measured with the digital ESDIAD/TOF detector and QMS/ESD detector. In Fig. 3, the total angle integrated $^{16}O^+$ yield obtained with a large angle of detection condition (+100 V sample bias) as a function of the overlayer coverage of NH_3 and $H_2{}^{18}O$ is shown on a semilogarithmic plot. It can be seen in Fig. 3 that the $^{16}O^+$ ion yields decrease exponentially as a function of NH_3 and $H_2{}^{18}O$ coverage; about 20% of the initial $^{16}O^+$ ions penetrate more than one monolayer of NH_3, whereas only 1% of the original $^{16}O^+$ ions are found to survive transmission of half a monolayer of $H_2{}^{18}O$.

In order to confirm the measurements made with the ESDIAD detector, the $^{16}O^+$ yield as a function of the overlayer coverage of NH_3 and $H_2{}^{18}O$ is measured with the QMS/ESD detector. We find that the $^{16}O^+$ attenuation measurements made with the QMS/ESD detector give the same results as the measurements made with the ESDIAD/TOF detector. These results imply that any changes in the angular distribution of the $^{16}O^+$ ions during passage through the molecular overlayers are small, because the acceptance angle of the QMS/ESD detector (~4°) is smaller than that of the ESDIAD (~22°). This is confirmed by the observations reported below.

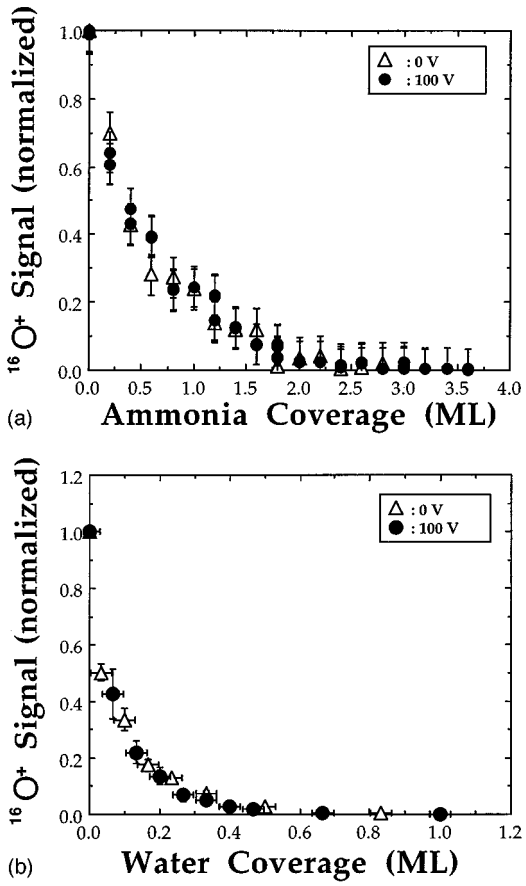

FIG. 4. Angle integrated $^{16}O^+$ yield for two different sample bias conditions as a function of (a) NH_3 and (b) $H_2{}^{18}O$ coverage. Close circles, 100 V sample bias and open triangles, 0 V sample bias. The data are normalized to 1 for the clean surface value.

In order to determine whether a measurable fraction of $^{16}O^+$ ions undergo large angle scattering, we compare the total angle integrated O^+ yield obtained with the small angle of detection condition (0 V sample bias) and with the large angle of detection condition (+100 V sample bias) using the ESDIAD/TOF detector. The total angle integrated $^{16}O^+$ yields obtained under these two conditions using the ESDIAD/TOF detector are depicted in Figs. 4(a) and 4(b) as a function of NH_3 and $H_2{}^{18}O$ coverage, respectively. It can be seen that there is no significant difference between both measurements. This result indicates that large angle (>22°) scattering of the O^+ ions is rare during their passage through the overlayers of NH_3 or $H_2{}^{18}O$.

Changes in the angular widths of the desorbing $^{16}O^+$ beam as a function of NH_3 and $H_2{}^{18}O$ overlayer thickness are shown in Figs. 5(a) and 5(b), respectively. The full-width at half-maximum (FWHM) of the $^{16}O^+$ ions increases slightly after traversing the NH_3 film. After traversing the $H_2{}^{18}O$ overlayer, the FWHM of $^{16}O^+$ ions first increases with increasing $H_2{}^{18}O$ coverage up to 0.2 ML, and then decreases. The increase in the FWHM of $^{16}O^+$ beam is indicative of small angle elastic forward scattering. The observed decrease

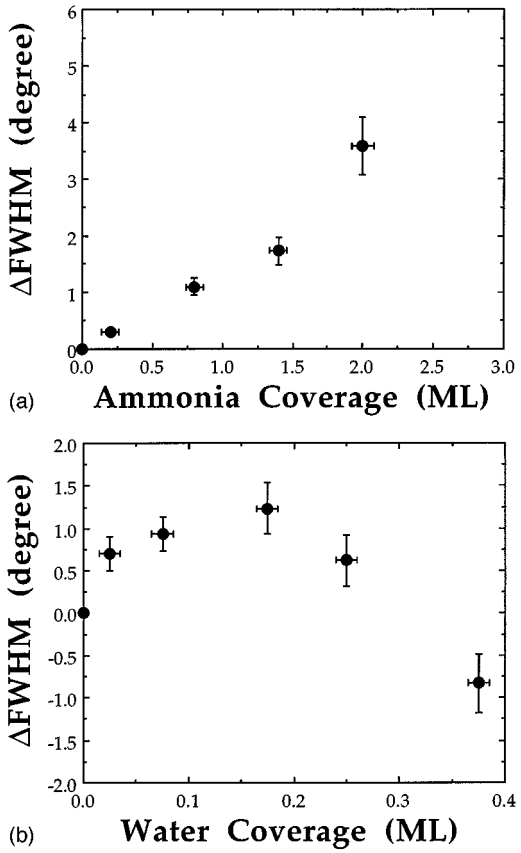

FIG. 5. Angular distribution, FWHM of $^{16}O^+$ beam as a function of (a) NH_3 and (b) $H_2{}^{18}O$ coverage (sample bias, 0 V).

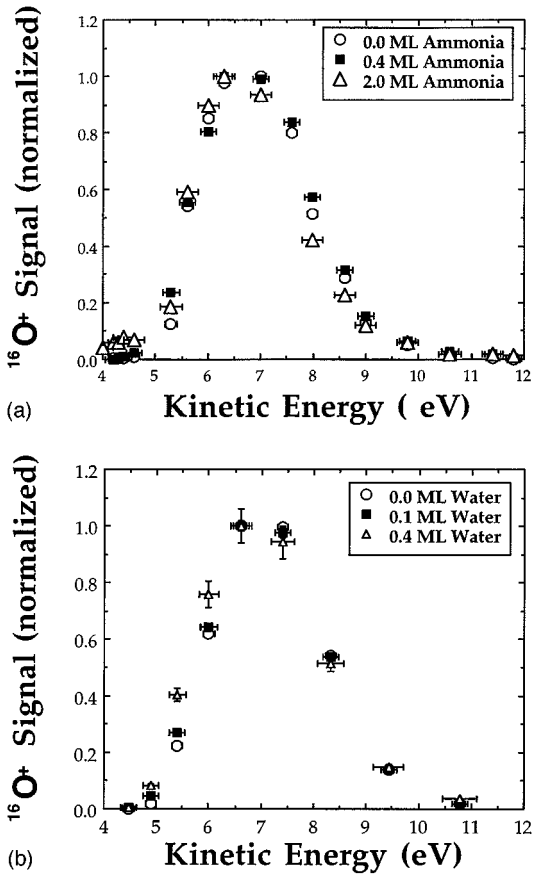

FIG. 6. Energy distribution of $^{16}O^+$ after passage through (a) NH_3 and (b) $H_2{}^{18}O$ of various coverage (sample bias, 0 V). Yields are normalized to unity at their maximum.

in the FWHM of $^{16}O^+$ beam after traversing the $H_2{}^{18}O$ overlayer (>0.2 ML) suggests either that the $^{16}O^+$ ions desorbing in slightly off-normal directions are attenuated stronger, or that the $H_2{}^{18}O$ overlayer focuses the ions toward the surface normal.

Using the ESDIAD/TOF detector, we analyze the energy distribution of the $^{16}O^+$ ions as a function of overlayer coverage. In order to transform a TOF spectrum $N(t)$ obtained in our measurement into an energy spectrum $N(E)$, constant time increments are converted into constant energy increments.[31] The energy E and the energy distribution $N(E)$ are obtained by

$$E=\frac{ML^2}{2t^2}, \tag{1}$$

$$N(E)=\frac{N(t)t^3}{ML^2}, \tag{2}$$

where L is the flight path and t is the measured time for an ion with mass M to travel from the substrate to the ESDIAD/TOF detector under field-free conditions. The FWHM of energy distribution of $^{16}O^+$ measured by using the ESDIAD/TOF detector from the clean oxidized W(100) surface is about 3 eV; this result is consistent with our retarding field measurement.[7] Figures 6(a) and 6(b) show the energy distribution of $^{16}O^+$ as a function of NH_3 and $H_2{}^{18}O$ coverage, respectively. Within the experimental uncertainty, there is no conclusive evidence for a shift in the energy distributions of the $^{16}O^+$ ions. However, the very small shifts to lower energies observed for ~2 ML of NH_3 and ~0.4 ML of $H_2{}^{18}O$ are consistent with elastic forward scattering.

Our ESD measurements show no direct evidence for products of ion–molecule chemical reactions, collision induced dissociation reactions and charge transfer reactions between the desorbing $^{16}O^+$ ions and overlayer molecules. We use the term *ion–molecule chemical reaction* to refer to a heavy particle rearrangement or associations such as $O^+ + NH_3 \rightarrow (NO)^+ + H_2 + H$. By *a charge-transfer reaction* we mean a reaction in which an electron is transferred between the two colliding particles, as in $O^+ + H_2O \rightarrow (H_2O)^+ + O$. Since for the energy range of interest (<10 eV), ionization by ion impact is not an important collision process, we do not consider ion-impact ionization collisions. Several different ion–molecule chemical reaction paths between a desorbing $^{16}O^+$ ion and a NH_3 molecule, and between a desorbing $^{16}O^+$ ion and a $H_2{}^{18}O$ molecule could be possible. For example, one would consider the reaction

$$^{16}O^+ + NH_3 \rightarrow (^{16}OH)^+ + NH_2 \tag{3}$$

and the reaction

$$^{16}O^+ + H_2{}^{18}O \rightarrow (^{16}OH)^+ + {}^{18}OH \tag{4}$$

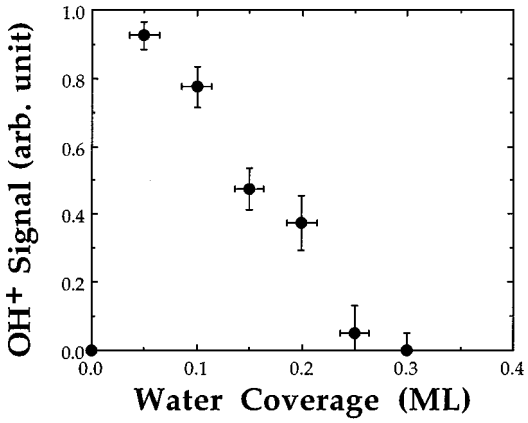

FIG. 7. Total ESD $(OH)^+$ yield from oxidized W(100) surface as a function of $H_2{}^{18}O$ coverage, obtained using QMS/ESD detector.

among the possible ion–molecule reaction paths. Since in our experiments, within the detectability limits $[(OH)^+/H^+<1\%]$, no $(OH)^+$ signal is observed from NH_3 adsorbed on the oxidized W(100) surface at any coverage, reaction (3) seems to be unlikely. However, after adsorption of 0.05 ML of $H_2{}^{18}O$ on the oxidized W(100) surface $(^{16}OH)^+$ and $(^{18}OH)^+$ signals are observed. Figure 7 shows the total $(OH)^+$ yield as a function of $H_2{}^{18}O$ coverage. It can be seen in Fig. 7 that the total $(OH)^+$ yield decreases as a function of $H_2{}^{18}O$ coverage. If the attenuation of $^{16}O^+$ emission was mainly due to the reaction (4), we would expect an increase in the total $(OH)^+$ yield, while the $^{16}O^+$ yield decreases as a function of $H_2{}^{18}O$ coverage. Therefore, the reaction (4) does not seem to be likely in our experiments. [As discussed earlier, we believe that the sources of $(OH)^+$ signals are the dissociation product of $H_2{}^{18}O$, OH species. The attenuation of ESD $(OH)^+$ ion emission as a function of $H_2{}^{18}O$ coverage is attributed to combination of one-electron charge transfer reactions and the formation of a hydrogen-bonded cluster $(OH–H_2O)$, as discussed in Ref. 19 in detail.]

Figure 8 shows QMS/ESD spectra from ~3 ML of NH_3 adsorbed on the oxidized W(100) surface; a similar spectra from ~0.5 ML of $H_2{}^{18}O$ adsorbed on the oxidized W(100) surface is found (see Ref. 19). In Fig. 8 only the ESD H^+ signal which originate from the overlayer molecules is seen; all other ion signals are suppressed. If an ion–molecule chemical reaction or a collision induced dissociation reaction were an important process in determining the attenuation of the $^{16}O^+$ emission, we would expect to see contributions from the reaction product ions in the spectra, yet adsorption of ~3 ML of NH_3 and ~0.5 ML of $H_2{}^{18}O$ on the oxidized W(100) surface suppress the $^{16}O^+$ emission almost completely.

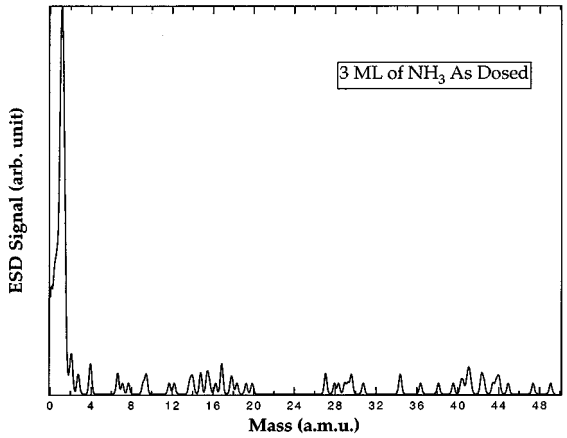

FIG. 8. ESD signals obtained using QMS/ESD detector from oxidized W(100) surface after adsorption of ~3 ML of NH_3 at 25 K.

IV. DISCUSSION

A. Adsorption of overlayers

The TDS measurements for NH_3 and $H_2{}^{18}O$ adsorbed on the oxidized W(100) surface at 25 K demonstrate that the majority of NH_3 and $H_2{}^{18}O$ adsorbed in the first monolayer remains molecular. As can be seen in Figs. 1(a) and 1(b), NH_3 and $H_2{}^{18}O$ monolayers desorb with peak temperatures of ~148 K and ~155 K, respectively. However, the TDS measurements imply that ~0.2 ML of NH_3 and ~0.08 ML of $H_2{}^{18}O$ dissociate. The TDS data, combined with ESD measurements using the QMS/ESD detector, indicate that a very small percentage of $H_2{}^{18}O$ dissociates upon adsorption to form adsorbed ^{16}OH and ^{18}OH. Since ESD with the ESD/QMS detector shows both $(^{16}OH)^+$ and $(^{18}OH)^+$ signals, we suggest that the dissociation of $H_2{}^{18}O$ is induced by ^{16}O and leads to OH species with different oxygen isotopes,

$$H_2{}^{18}O + {}^{16}O \rightarrow {}^{18}OH + {}^{16}OH. \tag{5}$$

Therefore, following the adsorption of $H_2{}^{18}O$, both $H_2{}^{18}O$ (predominantly for high coverages) and a small amount of OH species are present on the surface, and the transmission of $^{16}O^+$ ions can be affected by both $H_2{}^{18}O$ and OH species that are ESD active. Details of the dissociation of molecular $H_2{}^{18}O$ on the oxidized W(100) surface are discussed elsewhere.[19]

ESD of NH_3 adsorbed on oxidized W(100) surface produces only H^+ ions from the adsorbate for all coverages of NH_3. Therefore, we cannot conclude whether dissociation occurs upon adsorption or during the thermal desorption experiment. The ESD measurements made with the QMS/ESD detector are sensitive to $(OH)^+$. Since no ESD $(OH)^+$ signal is detected at any temperature or coverage for NH_3 adsorption, presumably dissociation does not lead to formation of OH species, or to the formation of OH species that do not produce an ESD $(OH)^+$ signal. {If NH_3 decomposition leads to the formation of lattice OH [OH(lat)], it may not produce an ESD $(OH)^+$ signal.} Román *et al.*[32] have reported that NH_3 adsorbs mainly molecularly at low coverages on perfect and defective $TiO_2(110)$ surfaces at 300 K. Recently, Diebold and Madey[29] have also reported that NH_3 adsorbs molecularly on $TiO_2(110)$. We speculate that the dissociation of a small amount of NH_3 on the oxidized W(100) surface may occur during thermal heating, but point out that if it occurs upon adsorption, no ESD-active OH is formed.

One of the characteristic features of the adsorption of water on a transition metal oxide surface is that water is not reported to form hydrogen-bonded clusters at low coverage.[33–35] Since we condense $H_2{}^{18}O$ at 25 K on the oxi-

dized surface, diffusion of $H_2{}^{18}O$ should be greatly hindered at 25 K; that is another reason why cluster formation at 25 K at fractional monolayer coverage is unlikely. Our ESD measurements reveal no significant change in the ESD signals from an oxidized W(100) surface covered with a fraction of a monolayer of NH_3 or $H_2{}^{18}O$ (see Ref. 19) in the temperature range of 25–120 K, indicating that the adsorbed molecules remain in their initial bonding sites in this temperature range. Therefore, based on the TDS and ESD results together, we suggest that $H_2{}^{18}O$ and NH_3 condensed at 25 K bond to specific tungsten-cation sites via the ^{18}O and N atoms, respectively.

B. Attenuation of $^{16}O^+$ ions

We now discuss the attenuation of $^{16}O^+$ ions by condensed molecular NH_3 and $H_2{}^{18}O$, and by their adsorbed dissociation products. The $^{16}O^+$ ion yields decrease exponentially as a function of NH_3 and $H_2{}^{18}O$ coverage, as seen in Fig. 3. We can derive an attenuation cross section of $^{16}O^+$, $\sigma_{\exp}$, using the equation

$$\phi = \phi_0 \exp(-\theta N_{\text{ads}} \sigma_{\exp}), \tag{6}$$

where ϕ and ϕ_0 are the total ion flux reaching the detector and the total ion flux desorbing from the clean oxidized W(100) surface, respectively, θ is coverage of NH_3 or $H_2{}^{18}O$ on the oxidized W(100) surface, and N_{ads} is the number of NH_3 or $H_2{}^{18}O$ molecules per cm^2. Using the derived number density of NH_3 and $H_2{}^{18}O$ on the oxidized W(100) surface (where 1 ML corresponds to $\sim 4.25\times10^{14}$ molecules/cm^2 for NH_3 and $\sim 8.5\times10^{14}$ molecules/cm^2 for $H_2{}^{18}O$) we can calculate the attenuation cross sections of $^{16}O^+$, $\sigma_{\exp}$, to be

$$\sigma_{\exp} = (3\pm1)\times10^{-15} \text{ cm}^2 \text{ for } NH_3$$

$$\sigma_{\exp} = (9\pm2)\times10^{-15} \text{ cm}^2 \text{ for } H_2{}^{18}O.$$

It is remarkable that half a monolayer of $H_2{}^{18}O$ is enough to suppress the $^{16}O^+$ emission almost completely and that the attenuation of $^{16}O^+$ is exponential even for such low coverages of $H_2{}^{18}O$. Recent work by Diebold and Madey suggests that charge transfer between O^+ and adsorbed NH_3 may be the dominant mechanism responsible for the suppression of ESD of O^+ ions from a $TiO_2(110)$ surface.[18] Our recent experimental observations on the transmission of low energy O^+ ions through ultrathin films of Ar, Kr, and Xe (Ref. 8) suggest that elastic scattering dominates for Kr and Xe films, but that charge transfer processes may also be important in causing attenuation of $^{16}O^+$ for Ar films. Molecular dynamics (MD) simulations that assume only elastic scattering performed by Klein, Vinanek, and Urbassek[36] are in good agreement with the experimental data for Kr and Xe. Along the same line, we suggest here a model in which charge transfer and elastic scattering are the main reasons for the attenuation of $^{16}O^+$ ions in the NH_3 and $H_2{}^{18}O$ overlayers on the oxidized W(100) surface.

Before discussing a charge transfer and elastic scattering attenuation model for the transmission of the $^{16}O^+$ ions through the overlayers, we first focus on other factors that may contribute to the observed attenuation of the $^{16}O^+$ ions.

1. Electron transport through overlayer and ESD mechanism

First, we consider the effect of the energy loss of the primary electron beam in the molecular overlayer on the ESD processes. The electron beam can cause excitations in the overlayer film, which results in energy loss of the electrons. In the gas phase, the total ionization cross sections of NH_3 and $H_2{}^{18}O$ for 300 eV electron impact are $\sim 2.1\times10^{-16}$ cm^2 and $\sim 1.6\times10^{-16}$ cm^2, respectively.[37–39] Using the total cross section data, we can derive an ionization mean free path for 300 eV electrons in NH_3 and $H_2{}^{18}O$ to be $\sim$20 Å. This result indicates that primary electrons having a kinetic energy of 300 eV have lost only a small fraction of their energy on their passage through the overlayer films, assuming an average energy loss per ionization of about 20 eV. Hence, the primary electrons have enough energy, even after losing some energy ($\sim$20 eV) in the overlayer, to cause an electronic excitation that leads to the desorption of the O^+ ions.[40,41] Since the ESD ion desorption cross section does not change significantly with primary electron energy in the range 100–300 eV,[42] we conclude that primary electron energy losses in the ultrathin overlayers do not affect the desorption probability of $^{16}O^+$.

The electronic excitations caused by the primary electron beam in the NH_3 and $H_2{}^{18}O$ overlayer films could lead to the ESD of molecular NH_3 and $H_2{}^{18}O$, ESD of H^+ ions and neutrals, as well as ionization. In addition, it is possible that secondary electrons generated as a result of the electron bombardment may also disturb the molecular overlayers electronically.[8,9] It is important to know the probability that an O^+ ion traverses through an area in the overlayer that is electronically disturbed by the primary electron beam (or by secondary electrons). Based on ESD measurements with an electron fluence of 2×10^{13} cm^{-2} from the molecular film covered surface, we derive an upper limit for a H^+ ion desorption yield on the order of 10^{-6} ions/electron; the oxygen ion desorption yield from the oxidized W(100) surface is on the order of 10^{-6} ions/electron.[43] In addition, we expect that other kinds of excitations such as vibrational-rotational and electronic excitations to form metastable molecules, may have several orders of magnitude higher excitation probability than the H^+ desorption probability. The estimated $^{16}O^+$ ion desorption yield and expected total electronic excitation probability in the overlayer film indicate that the probability of an O^+ traversing an electronically disturbed area in the overlayer film is very low. Therefore, we do not think that disturbance of the molecular film by primary electrons (or by secondary electrons) is a significant problem affecting the measured parameters.

We also consider that elastic back scattering of primary electrons from the overlayers may have an influence on the attenuation of $^{16}O^+$. It is well known that the electron elastic forward scattering amplitude from a surface depends strongly on the primary electron kinetic energy;[44] the amplitude of forward peaking in the elastic scattering probability increases with increasing electron kinetic energy. For an electron having a kinetic energy of $\sim$300 eV, very low scattering amplitudes at large scattering angles are observed. Therefore, we consider that elastic backscattering of primary

electrons from the overlayers is not an important factor in our experiments and does not significantly affect the attenuation of $^{16}O^+$.

It is possible that the presence of overlayer molecules on the surface may cause a change in the local electronic structure, and this electronic change may affect the $^{16}O^+$ ion desorption probability and influence the $^{16}O^+$ attenuation. We can obtain some information about the strength of the adsorbate–substrate bond from the TDS data.[26] As shown in Figs. 1(a) and 1(b), NH_3 and $H_2{}^{18}O$ monolayer desorption from oxidized W(100) takes place at around 150 K. This observation indicates that there is only a very weak chemical interaction (~0.4–0.5 eV) between the substrate and NH_3 or $H_2{}^{18}O$. Using ultraviolet photoelectron spectroscopy (UPS) Kurtz *et al.*[35] have shown that molecularly adsorbed H_2O on a TiO_2 (110) surface at 160 K does not influence substantially the substrate electronic structure. Diebold and Madey[18] have recently argued that based on x-ray photoemission spectra (XPS) and UPS, the adsorption of NH_3 on TiO_2 (110) has little affect on the substrate electronic structure. Thus, it is unlikely that the presence of the overlayer of NH_3 or $H_2{}^{18}O$ changes the substrate electronic structure enough to affect the ion desorption probability from the oxidized surface, or to cause the observed attenuation of $^{16}O^+$. However, even though the bonding interaction is weak, the presence of the overlayers may have an influence on the lifetime and the electronic structure of the final states that determine the ion desorption probability. Below we discuss more the possible influence of the overlayers on the $^{16}O^+$ desorption in terms of ion desorption and charge transfer mechanisms.

As discussed earlier, a very small fraction of $H_2{}^{18}O$ dissociates upon adsorption to form OH species. As discussed in detail in Ref. 19, the $H_2{}^{18}O$ dissociation product OH species are gone from the surface at ~350 K. This result shows that there is a chemisorption bond between the substrate and OH. This bonding may be accompanied by charge transfer between the substrate and OH, because adsorbed OH is an electron acceptor. The charge transfer may effect the local electronic structure and the ion desorption. However, because the maximum concentration of dissociated species is small, and because attenuation data extend to high coverages, we do not believe this affects our interpretation of σ_{exp} significantly. Moreover, since there is no change in attenuation rate from low to high coverages, this also is an argument against a strong influence of adsorption on the initial excitations. It can be seen in Fig. 3 that no changes in slopes are observed from a fraction of a monolayer to multilayers for NH_3 and from ~0.1 ML (OH) to 1 ML ($H_2{}^{18}O$) for $H_2{}^{18}O$. Therefore, we believe that the exponential attenuation of $^{16}O^+$ emission upon adsorption of molecular NH_3 and $H_2{}^{18}O$ are mainly due to collisions (elastic and/or inelastic) between desorbing $^{16}O^+$ ions and NH_3 molecules, and between $^{16}O^+$ ions and $H_2{}^{18}O$ molecules.

In summary, molecular NH_3 and $H_2{}^{18}O$ interact with the oxidized W(100) weakly, and no significant change in the WO_{2-3} surface electronic structure is expected. We do not expect that the presence of a weakly interacting molecular overlayer has a strong affect on the initial excitation processes leading to desorption of O^+ ions. However, the dissociated species (e.g., OH) are chemisorbed and may affect the local density of states.

2. Inelastic energy transfer processes

ESD produced $^{16}O^+$ ions, in their passage through the NH_3 and $H_2{}^{18}O$ overlayers, can collide with the overlayer molecules through various elastic and inelastic processes, such as elastic, electronic, and vibrational energy transfer, and charge transfer. During an ion–molecule collision energy can be transferred among rotational, vibrational, electronic, and translational degrees of freedom,[45] depending on the relative energy of collision. In one-electron charge transfer reaction which has been suggested as a dominant ion attenuation process,[18] an incident ion picks up an electron from a target atom or molecule, and becomes neutral. Ion–molecule charge transfer reactions are significantly different from ion–atom charge transfer reaction, because the vibrational and rotational energy levels of molecules play additional roles during ion–molecule charge transfer reactions.[45,46]

Let us now consider inelastic (electronic, vibrational, and rotational) energy transfer processes during the transmission of the $^{16}O^+$ ions through the NH_3 and $H_2{}^{18}O$ overlayers. Since electronic excitation energies are typically above 1 eV, electronic energy transfer is quite inefficient in the low energy (<10 eV) ion–molecule reactions. Therefore, we expect that electronic excitations in the overlayers by ~7 eV $^{16}O^+$ are unlikely.[45] Furthermore, for collisions with large impact parameters (and small scattering angles), the inelastic energy transfer processes cannot be efficient;[45] these collisions are more elastic. Our measured $^{16}O^+$ attenuation cross sections for NH_3 ($\sim 3\times10^{-15}$ cm^2) and $H_2{}^{18}O$ ($\sim 9\times10^{-15}$ cm^2) imply that the $^{16}O^+$–NH_3 and $^{16}O^+$–$H_2{}^{18}O$ collision distances are very large. These indicate that the electronic and vibrational-rotational excitations are inefficient by the surviving ions. As seen Figs. 6(a) and 6(b), the energy distributions of the $^{16}O^+$ ions after traversing the overlayer films show no significant change within the experimental uncertainty, indicating that the inelastic energy losses are not important. However, the very small shift in the energy distributions of the $^{16}O^+$ ions are consistent with the very small change in the angular distributions of the $^{16}O^+$ ions [see Figs. 5(a) and 5(b)] due to elastic forward scattering.

3. Attenuation model

We now suggest an attenuation model for $^{16}O^+$ ions passing through the NH_3 and $H_2{}^{18}O$ overlayers in which the attenuation is caused by a combination of charge transfer (c.t.) and elastic scattering (e.s.) interactions of the $^{16}O^+$ ions with the NH_3 and $H_2{}^{18}O$ overlayers,

$$\sigma_{exp} = \sigma_{c.t.} + \sigma_{e.s.}. \tag{7}$$

a. Elastic scattering: The experimental results shown in Figs. 4(a) and 4(b) for the attenuation of $^{16}O^+$ in the NH_3 and $H_2{}^{18}O$ overlayers indicate that large angle elastic scattering is not a dominant process that causes the strong attenuation of $^{16}O^+$. In the following we discuss the possible contributions of elastic scattering to the attenuation of $^{16}O^+$ in the NH_3 and $H_2{}^{18}O$ overlayers.

Not every elastic scattering event of $^{16}O^+$ causes the attenuation of $^{16}O^+$ ions. Only those $^{16}O^+$ ions that are elastically backscattered or scattered with such a large angle that they cannot escape from the surface are attenuated. If $^{16}O^+$ ions are scattered in a forward direction through the overlayers so that they can escape from the surface (desorb), we can detect them in our experiment.

It can be seen in Figs. 4(a) and 4(b) that the angle integrated $^{16}O^+$ yield as a function of overlayer obtained with the small angle of detection condition is not significantly different from that obtained with the large angle of detection condition. This observation suggests that the $^{16}O^+$ ions are not scattered by large angles in the forward direction. Our earlier studies of the transmission of O^+ ion through Xe overlayer reveals evidence for large angle forward scattering; the measured attenuation cross section obtained from measurements made with 0 V sample bias is significantly different from that obtained with +100 V sample bias and an energy loss is observed in ion energy distributions.[8] We have attributed the attenuation of $^{16}O^+$ in Xe films to be due mainly to elastic backscattering. The large angle forward scattering and energy loss is an indicator that elastic scattering occurs. This observation is confirmed by MD simulations.[36] Since no large angle scattering of $^{16}O^+$ in the NH_3 and $H_2{}^{18}O$ overlayer is observed, we believe that backscattering of $^{16}O^+$ ions in the NH_3 and $H_2{}^{18}O$ overlayer is not a dominant process.

Furthermore, since NH_3 and $H_2{}^{18}O$ have very nearly the same mass and similarly large dipole moments, if elastic scattering were a dominant attenuation process, one would expect very similar $^{16}O^+$ attenuation cross sections for both NH_3 and $H_2{}^{18}O$. Therefore, we conclude that the observed attenuation of the $^{16}O^+$ ions cannot be explained primarily by backscattering and large angle elastic scattering alone.

The observed increase in angular distribution and slight shift in energy distribution of $^{16}O^+$ ions after traversing the overlayer films under field free conditions indicate that some $^{16}O^+$ ions are slightly scattered in the forward direction, as seen in Fig. 5, and Fig. 6. The maximum increases in angular FWHM are approximately 4° for NH_3 and 1° for $H_2{}^{18}O$ overlayer. For Gaussian widths, α, we calculate the broadening in angular FWHM using the following relation:

$$\alpha_{\text{final}}^2 \approx \alpha_{\text{initial}}^2 + \alpha_{\text{broadening}}^2, \tag{8}$$

where α_{initial} is the FWHM of the $^{16}O^+$ ion beam from the clean surface and α_{final} is the FWHM of the $^{16}O^+$ ion beam after traversing the overlayers. These calculations indicate that the increases in FWHM correspond to a maximum broadening of ~11° for the NH_3 overlayer and ~5° for the $H_2{}^{18}O$ overlayer. Since $H_2{}^{18}O$ and NH_3 have very large dipole moments (1.4×10^{-18} esu cm for NH_3 and 1.85×10^{-18} esu cm for $H_2{}^{18}O$), one expects small angle scattering of $^{16}O^+$ from NH_3 and $H_2{}^{18}O$ for very large impact parameter.

We can calculate the angular deflection of $^{16}O^+$ ion during collision with a single NH_3 molecule or $H_2{}^{18}O$ by using an ion-polar molecule potential function to compare the observed change in the angular distribution with the results of a theoretical calculation. We choose a potential function that includes both a long range charge-induced dipole potential and an ion-dipole potential,

$$V(r) = -\frac{e^2\alpha}{2r^4} - \frac{\mu_D e}{r^2}\cos\varphi, \tag{9}$$

where α is the dipole polarizability, μ_D is the permanent dipole moment of the neutral molecule, and φ is the angle that the dipole makes with the line of centers of the collision.[47] Tables I and II list the calculated scattering angles of a 7 eV $^{16}O^+$ ion from NH_3 and $H_2{}^{18}O$, respectively, as a function of impact parameter for different φ. As seen in Tables I and II, the calculated impact parameters for a wide range of β (scattering angle) values are larger than ~3 Å for ~11° scattering (for NH_3) and ~4 Å for ~5° scattering (for $H_2{}^{18}O$). Hence, the calculated results, the experimentally observed very small changes in the angular distributions, and also the lack of large angle forward scattering of $^{16}O^+$ during their passage through the NH_3 and $H_2{}^{18}O$ overlayer indicate that any elastic collision between O^+ and the molecular overlayers occurs with only large impact parameter.

We can also calculate the energy loss, δE, of a 7 eV $^{16}O^+$ in a collision with NH_3 or $H_2{}^{18}O$, leading to very small angle scattering,

$$\delta E = E_0\left\{1 - \left[\frac{(m_{\text{mol}}^2 - m_{0^+}^2\sin^2\beta)^{1/2} + m_{0^+}\cos\beta}{m_{\text{mol}} + m_{0^+}}\right]^2\right\}, \tag{10}$$

where m_{mol} is the mass of the target molecule (NH_3 or $H_2{}^{18}O$) and β is the scattering angle. Tables III and IV list the

TABLE I. Calculated scattering angle as a function of impact parameter for various dipole-ion angles, φ, for O^+–NH_3 collision. See text for details.

Impact parameter b (Å)	Scattering angle, β (deg)			
	φ=0°	φ=30°	φ=45°	φ=60°
2.5	21.8	19.9	17.7	14.9
3.0	11.5	10.4	9.2	7.6
3.5	7.2	6.5	5.7	4.6
4.0	5.0	4.5	3.9	3.1
4.5	3.7	3.3	2.8	2.2
5.0	2.9	2.6	2.2	1.7
5.5	2.3	2.1	1.7	1.3
6.0	1.9	1.7	1.4	1.1

TABLE II. Calculated scattering angle as a function of impact parameter for various dipole-ion angle, φ, for O^+–$H_2{}^{18}O$ collision. See text for details.

Impact parameter b (Å)	Scattering angle, β (deg)			
	φ=0°	φ=30°	φ=45°	φ=60°
2.5	20.7	18.0	15.8	12.6
3.0	11.8	10.2	8.9	7.0
3.5	7.8	6.7	5.8	4.5
4.0	5.6	4.8	4.1	3.1
4.5	4.3	3.6	3.1	2.3
5.0	3.4	2.9	2.5	1.8
5.5	2.8	2.3	2.0	1.5
6.0	2.3	2.0	1.7	1.2

TABLE III. Calculated energy of loss of 7 eV O^+ during the elastic collision with NH_3 molecule as a function of a scattering angle.

Scattering angle β (deg)	Energy loss δE (eV)
1.0	0.00
2.0	0.01
3.0	0.02
4.0	0.03
5.0	0.05
6.0	0.07
7.0	0.18
8.0	0.13
9.0	0.16
10.0	0.20
11.0	0.24
12.0	0.29
20.0	0.77

energy loss as a function of scattering angle in the range from 1° to 20°; the calculated energy loss for very small angle scattering is almost negligible. The observation of very little shift to lower energies in the energy distribution of $^{16}O^+$ as a function of the overlayer coverage [Figs. 6(a) and 6(b)] is in good agreement with the calculated energy loss results for small angle scattering. Therefore, our measured angular and energy distributions of the $^{16}O^+$ ions together indicate very small angle elastic scattering of $^{16}O^+$ in the NH_3 and $H_2{}^{18}O$ overlayer.

From the measured attenuation cross section for the NH_3 and $H_2{}^{18}O$ overlayers, we can estimate the attenuation collision radius, R_{acr}, leading to the attenuation of the $^{16}O^+$ by assuming that $\sigma_{\mathrm{exp}} \approx \pi R_{\mathrm{acr}}^2$. We calculate $R_{\mathrm{acr}} \approx 3$ Å for the NH_3 overlayer and $R_{\mathrm{acr}} \approx 5.3$ Å for the $H_2{}^{18}O$ overlayer. These estimated attenuation collision radii are too large to be realistic for elastic backscattering and large angle scattering, for which smaller impact parameters are necessary, and explain why only small angle scattering, for which larger impact parameters are necessary, is observed. The calculated impact parameters ($\sim$3 Å for NH_3, $\sim$4 Å for $H_2{}^{18}O$) are slightly smaller than the estimated attenuation radii. Although in the calculations we consider only the interaction between a single molecule and an ion, the estimated attenuation collision radii are in fairly good agreement with the calculated impact parameters for small angle scattering.

TABLE IV. Calculated energy of loss of 7 eV O^+ during the elastic collision with $H_2{}^{18}O$ molecule as a function of scattering angle. See text for more details.

Scattering angle β (deg)	Energy loss δE (eV)
1.0	0.00
2.0	0.01
3.0	0.02
4.0	0.03
5.0	0.04
6.0	0.06
7.0	0.08
8.0	0.11
9.0	0.14
10.0	0.17
11.0	0.21
12.0	0.24
20.0	0.66

From the measured angular and energy distribution of the $^{16}O^+$ ions as a function of the NH_3 and $H_2{}^{18}O$ overlayer thickness, we conclude that elastic scattering of the desorbing ions is not a dominant process in the attenuation of the $^{16}O^+$ ions. The very small changes in the angular and the energy distribution of the desorbing $^{16}O^+$ ions, and the lack of large angle and backscattering suggest that another process having a larger cross section than the elastic scattering cross section dominates over elastic scattering, so that no large angular forward scattering is observed.

b. Charge transfer: Since we conclude that backscattering and large angle elastic scattering alone cannot explain the $^{16}O^+$ attenuation, we must consider inelastic processes. The strong attenuation of the $^{16}O^+$ ions in the NH_3 overlayer, and especially in the $H_2{}^{18}O$ overlayer, suggests that ion–molecule charge transfer reactions, chemical reactions, and collision induced dissociation reactions,[18,45,46,48] between an $^{16}O^+$ ion and overlayer molecules, could be the dominant attenuation processes. Ion–molecule charge transfer, chemical and collision induced dissociation reactions depend strongly on internal energy of the collision partners and the relative collision energy. The different mechanisms depend also on the collision impact parameter and the orientation of the molecules during the collision.

In a one-electron charge transfer reaction an O^+ ion captures an electron from a target molecule and becomes a neutral. Since a charge transfer reaction does not necessarily involve direct momentum transfer, the desorption of $(NH_3)^+$ or $(H_2{}^{18}O)^+$ (which are expected charge transfer reaction products) as a result of the charge transfer collision is unlikely, and we do not detect them. As discussed in Sec. III C, our measurements show no direct evidence for any kind of ion–molecule chemical reaction or collision induced dissociation reaction. Since ion–molecule charge transfer reactions generally have large cross sections (10^{-14}–10^{-15} cm^2) at low energies (<10 eV) for exothermic reactions, we focus on charge-transfer processes.

Charge-transfer reactions between ions and atoms or molecules play important roles in many diverse areas such as gaseous discharges, electrochemistry, astrophysics, and surface science, and provide an understanding for nonadiabatic processes involving multiple potential energy surfaces.[49–51] Ion–molecule charge transfer collisions are significantly different from ion–atom charge transfer collisions, since in ion–molecule charge transfer reactions, at least one of the collision partners is a molecule, the vibrational and rotational excitations may come into play during charge transfer reactions. Recent experimental studies have shown that the vibrational and rotational states of the collision partners play very important roles in ion–molecule charge transfer reactions.[45,46,48]

In a charge-transfer reaction, the energy defect (ionization energy difference between interacting ion and neutral, at infinite separation) is a very important parameter, and provides intuitive knowledge about the reactions.[52] For ex-

ample, assuming values of ionization potentials for free atomic oxygen (~13.6 eV) and gaseous NH_3 (~10.17 eV) and H_2O (~12.61 eV) and if we consider only the ground states, the energy defects are ~2.2 eV for the nonresonant charge transfer reaction

$$O^+ + (NH_3) \rightarrow O + (NH_3)^+, \tag{11}$$

~1 eV for the nonresonant charge transfer reaction

$$O^+ + H_2O \rightarrow O + (H_2O)^+, \tag{12}$$

and ~0.4 eV for the nonresonant charge transfer reaction

$$O^+ + OH \rightarrow O + (OH)^+; \tag{13}$$

these reactions are all exothermic. At low collision energy (<10 eV), the charge transfer cross section depends strongly on whether a reaction is exothermic or endothermic.[53] Since reactions (11), (12), and (13) are all exothermic, we expect that the charge-transfer reactions are important inelastic collision channels determining the attenuation of $^{16}O^+$ through the molecular overlayers.

Experimental and theoretical studies on charge transfer in gas phase collisions indicates that the smaller the energy defect, the larger the charge transfer probability.[52] Based on the energy defect, one expects for the same relative collision energy that the charge transfer cross section would be largest for the O^+–(OH) collision and smallest for the O^+–(NH_3) collision. Furthermore, at low energies an ion-neutral (atom or molecule) interaction can best be viewed as involving transitions between a set of quasimolecular electronic states formed by the colliding ion and neutral. Although in some cases, like the O^+–NH_3 reaction (~2.2 eV), the energy defect may be large between colliding partners, at small internuclear separations potential energy curves of quasimolecules may cross or come so close that a transition from one state to another becomes possible, and this may result in a charge transfer collision. It can be envisioned that at small internuclear separations, the outer electrons may move in the field of the two charge centers. Therefore, a charge-transfer collision occurs when an ion and a neutral come so close together that their outer electrons have a significant probability of following either nucleus out.

The electron transfer can be accomplished during the time of the order of characteristic period of motion of the electron in an atom; the characteristic charge transfer transition time is $\tau_0 \approx 10^{-15}$ s.[45] When the collision time, τ_c, is approximately equal to the characteristic time, the transition probability is expected to peak.

The collision time (or lifetime), τ_c, is defined as $\sim(a/\nu)$, where a is the range of the interaction and ν is the relative collision velocity.[45] For the $^{16}O^+$–NH_3 and $^{16}O^+$–$H_2{}^{18}O$ collisions, we can equate a to the attenuation collision radius, R_{acr}, ($R_{acr} \approx 3$ Å for $^{16}O^+$–NH_3 collision and $R_{acr} \approx 5.3$ Å for $^{16}O^+$–$H_2{}^{18}O$ collision). For ~7 eV $^{16}O^+$ ion ($\nu \cong 9.2\times10^5$ cm/s), we can calculate the collision time as $\sim 3\times10^{-14}$ s for the $^{16}O^+$–NH_3 reaction and $\sim 6\times10^{-14}$ s for the $^{16}O^+$–$H_2{}^{18}O$ reaction. Comparison of these calculated collision times with the characteristic charge-transfer time ($\sim 10^{-15}$ s) shows that the charge transfer reaction for both $^{16}O^+$–NH_3 and $^{16}O^+$–$H_2{}^{18}O$ collisions is a likely interaction channel.

Hasted[54] has derived values of a (interaction range) from the observed positions of the cross section maxima for nonresonant one-electron charge-transfer. He has shown that a is quite large, ~7 Å, for a large number of experimental data. Since our calculated values of R_{acr} for $^{16}O^+$–NH_3 and $^{16}O^+$–$H_2{}^{18}O$ reactions are of comparable magnitude to Hasted's values, the charge-transfer reaction seems to be a very important process for both $^{16}O^+$–NH_3 and $^{16}O^+$–$H_2{}^{18}O$ collisions.

Let us now compare our experimental attenuation cross sections with one-electron charge transfer cross sections between O^+ and NH_3, and O^+ and H_2O in the gas phase. There are no experimental data available in the $^{16}O^+$ ion kinetic energy range 4 eV$<E_k<$10 eV; the only available data for the systems of interest are in the thermal energy range. For the charge-transfer reaction

$$O^+ + NH_3 \rightarrow O + (NH_3)^+ \tag{14}$$

and the charge-transfer reaction

$$O^+ + H_2O \rightarrow O + (H_2O)^+, \tag{15}$$

the rate coefficients at room temperature measured using the selected ion flow tube method are 1.2×10^{-9} cm^3/ (molecules s) and 3.2×10^{-9} cm^3/(molecules s), respectively.[55,56] These experimental gas phase rate coefficients can be converted into cross sections of $\sim 2.2\times10^{-14}$ cm^2 for the O^+–NH_3 charge-transfer reaction and $\sim 5.8\times10^{-14}$ cm^2 for the O^+–H_2O charge-transfer reaction. As mentioned earlier, the charge-transfer reactions depend strongly on the relative collision energy; the charge-transfer cross sections for ion–molecule reactions are generally larger at thermal energies.[46] We expect that the charge transfer cross sections for these reactions at higher energies (1–10 eV) are several order of magnitude smaller than that of thermal energies. It is very encouraging that both the gas phase data at thermal energies and our experimental results for ~7 eV O^+ show the same trend, that is *the O^+–H_2O cross section ($\sim 9\times10^{-15}$ cm^2) is approximately three times larger than the O^+–NH_3 cross section ($\sim 3\times10^{-15}$ cm^2).*

It is helpful to compare the experimental results with the results of the most commonly utilized theoretical models; the Langevin ion-induced dipole theory[47] and average dipole orientation (ADO) theory.[47,56] Table V compares the experimental rate coefficients with the theoretical predicted rate coefficients for the O^+–NH_3 and O^+–H_2O charge-transfer reactions. It can be seen in Table V that neither the Langevin nor ADO theories predict relative rate coefficients (cross sections) at thermal energies correctly for these reactions. Furthermore, both Langevin and ADO theories estimate cross sections for ion–molecule reaction very poorly at high energy (>1 eV). Therefore, we cannot compare our experimental results with the theoretical cross sections.

Our measured attenuation cross section ($\sim 3\pm1\times10^{-15}$ cm^2) for the interaction of 7 eV $^{16}O^+$ with NH_3 is in good agreement with the attenuation cross section ($2.8\pm0.5\times10^{-15}$ cm^2) measured by Diebold and Madey[18] for

TABLE V. Experimental and theoretical predicted cross sections for O^+–NH_3 and O^+–H_2O one-electron charge-transfer reactions at thermal energies and at ~7 eV.

	Cross section at thermal energy (~0.025 eV)			Cross section at ~7 eV
Reaction	Langevin (cm^2)	ADO[a] (cm^2)	Experimental[a] (cm^2)	Experimental[b] (cm^2)
O^+–NH_3	$\sim 2.2\times10^{-14}$	$\sim 4.0\times10^{-14}$	$\sim 2.2\times10^{-14}$	$\sim 3\times10^{-15}$
O^+–H_2O	$\sim 1.7\times10^{-14}$	$\sim 4.4\times10^{-14}$	$\sim 5.8\times10^{-14}$	$\sim 9\times10^{-15}$

[a]Reference 57.
[b]In the present study.

the interaction of 5 eV $^{16}O^+$ with adsorbed NH_3. They have measured the transmission of O^+ ions as a function of coverage up to the saturation coverage of chemisorbed NH_3 on a TiO_2(110) surface, and they have found a linear attenuation of O^+ ions. Our measurement made at 25 K up to a very high coverage of NH_3 shows an exponential attenuation of O^+ ions in thicker NH_3 overlayers. Moreover, the two measurements behave nearly the same up to the saturation coverage of chemisorbed NH_3. Thus, we argue that to within experimental uncertainty our measured cross section shows good agreement with the measured cross section by Diebold and Madey. Note that Diebold and Madey have used an entirely different apparatus. Measuring very similar attenuation behavior for $^{16}O^+$ ion through NH_3 by using two different substrates [TiO_2(110) and oxidized W(100) surface] indicates that there is almost no substrate dependence of ion attenuation by ultrathin films. This supports our model that the attenuation of ^{16}O by the NH_3 overlayer is mainly due to charge-transfer between $^{16}O^+$ and NH_3.

We attribute the strong attenuation of $^{16}O^+$ by the $H_2{}^{18}O$ overlayer to be mainly due to charge-transfer between $^{16}O^+$ and OH, and between $^{16}O^+$ and $H_2{}^{18}O$. As mentioned earlier, the energy defects for the $^{16}O^+$–OH and the $^{16}O^+$–$H_2{}^{18}O$ reactions are 0.4 and 1.0 eV, respectively, and both are exothermic. Based on the values of the energy defects, we expect that the charge-transfer cross section between $^{16}O^+$ and OH is larger than that between $^{16}O^+$ and $H_2{}^{18}O$. We suggest that the very strong decrease of the $^{16}O^+$ yield in the coverage range of 0–0.1 ML of $H_2{}^{18}O$ (about 0.08 ML of $H_2{}^{18}O$ dissociates) is mainly due to charge-transfer between $^{16}O^+$ and OH. However, we can not exclude some electronic influence of chemisorbed OH species on the initial $^{16}O^+$ desorption.

Based on the observed attenuation of $^{16}O^+$, we conclude that charge transfer between the $^{16}O^+$ ions desorbing from the oxidized W(100) surface and the adsorbed molecules, $H_2{}^{18}O$, OH, and NH_3, are the dominant processes determining the depth of origin of desorbing $^{16}O^+$ ions.

The transmission of the $^{16}O^+$ ions through the NH_3 overlayer can be explained by Poisson statistics of the collisions.[8,9] When the oxidized W(100) surface at 25 K is exposed to NH_3, NH_3 molecules strike the surface at random positions and may stay close to the sites where they landed, because the diffusion of molecule is greatly hindered at 25 K. This leads to a statistical growth mode. As discussed earlier, however, the NH_3 molecules in the first monolayer may be adsorbed at specific surface cation sites. We expect that the first monolayer growth of the NH_3 films may lead to a very small deviation from the functional form of the attenuation. The exponential attenuation of $^{16}O^+$ ions in the NH_3 overlayer indicates that our system can be described by Poisson statistics; the NH_3 overlayer grows almost statistically and binary collisions are the dominant collision processes.

Since only a fraction of a monolayer of $H_2{}^{18}O$ leads to the exponential attenuation of $^{16}O^+$ ions, we cannot explain the attenuation of $^{16}O^+$ ions in the $H_2{}^{18}O$ overlayer based solely on Poisson statistics of the collisions. However, the exponential attenuation of $^{16}O^+$ ions in their passage through the $H_2{}^{18}O$ overlayer is supported by a geometrical model. We speculate that with increasing $H_2{}^{18}O$ coverage the effective interaction area of neighboring $H_2{}^{18}O$ molecules overlap, because the effective interaction area ($R_{acr}\approx 5.3$ Å) is much larger than the molecular size of $H_2{}^{18}O$ ($R_{water}\approx 1.45$ Å). Therefore, a linear decrease of the $^{16}O^+$ ion yield with increasing number of $H_2{}^{18}O$ molecules is not observed. Based on this argument, we believe that the possible overlap in the effective interaction area of $H_2{}^{18}O$ molecules leads to the observed exponential attenuation of $^{16}O^+$ starting at the lowest coverage.

V. CONCLUSIONS

We have developed a novel experimental approach to study the charge-transfer and energy transfer processes that occur in the desorption of ESD produced low energy ions below an overlayer film. In this study, we have shown that the $^{16}O^+$ signal is attenuated to ~1% by 3 ML of NH_3 and 0.5 ML of $H_2{}^{18}O$. We have attributed the attenuation of the ions in the overlayer films mainly to one-electron charge-transfer between $^{16}O^+$ and the condensed molecular species. Other elastic and inelastic processes are not believed to contribute significantly to $^{16}O^+$ attenuation in NH_3 and $H_2{}^{18}O$ films. Our experimental results reveal that the overlayer electronic and chemical properties play very important roles in the desorption of ions created below the overlayers. Our measurements also indicate no substrate dependence of the ion attenuation by ultrathin films.

In order to develop a better understanding of the dominant processes in the desorption of ions created below the overlayer films, in future investigations, we will study transmission of a variety of ions, such as F^+, F^-, H^+, Cl^+, Cl^-, and O^- through rare gases and molecular overlayers.

ACKNOWLEDGMENTS

N.J.S. acknowledges partial support from the Alexander-von-Humboldt foundation. This work has been supported in part by the National Science Foundation, Grant No. CHE-9408367.

[1] T. E. Madey, Science **234**, 316 (1986).
[2] R. G. Ramsier and J. T. Yates, Jr., Surf. Sci. Rep. **12**, 243 (1991).
[3] P. Sigmund, M. T. Robinson, and M. S. Baskes, Nucl. Instrum. Methods Phys. Res. B **36**, 110 (1989).
[4] J. W. Burnett, J. P. Biersack, D. M. Gruen, B. Jorgensen, A. R. Krauss, M. J. Pellin, E. L. Schweitzer, J. T. Yates, Jr., and C. E. Young, J. Vac. Sci. Technol. A **6**, 2064 (1988).
[5] W. L. Brown, Phys. Rev. B **32**, 1988 (1988).
[6] M. McCartney and D. Smith, Surf. Sci. **221**, 214 (1989).
[7] N. J. Sack, M. Akbulut, and T. E. Madey, Nucl. Instrum. Methods Phys. Res. B **90**, 451 (1994).
[8] N. J. Sack, M. Akbulut, and T. E. Madey, Phys. Rev. Lett. **73**, 794 (1994).
[9] N. J. Sack, M. Akbulut, and T. E. Madey, Phys. Rev. B **51**, 4585 (1995).
[10] P. Nordlander and J. C. Tully, Phys. Rev. Lett. **61**, 990 (1988).
[11] P. Nordlander, Scanning Microsc. Suppl. **3**, 353 (1990).
[12] J. C. Tully, Phys. Rev. B **16**, 4324 (1977).
[13] M. L. Yu and N. D. Lang, Nucl. Instrum. Methods Phys. Res. B **14**, 403 (1986).
[14] P. Avouris and R. E. Walkup, Annu. Rev. Phys. Chem. **40**, 173 (1989).
[15] S. A. Joyce, C. Clark, V. Chakarian, D. K. Shuh, J. A. Yarmoff, T. E. Madey, P. Nordlander, B. L. Maschhoff, and H. S. Tao, Phys. Rev. B **45**, 14 264 (1992).
[16] T. E. Madey, S. E. Joyce, and C. Benndorf, in *Physics and Chemistry of Alkali Metal Adsorption*, edited by H. P. Bonzel, A. M. Bradshaw, and G. Ertl (Elsevier, New York, 1989), p. 185.
[17] F. P. Netzer and T. E. Madey, J. Chem. Phys. **76**, 710 (1982).
[18] U. Diebold and T. E. Madey, Phys. Rev. Lett. **72**, 1116 (1994).
[19] M. Akbulut, N. J. Sack, and T. E. Madey, Surf. Sci. (accepted).
[20] D. A. King, T. E. Madey, and J. T. Yates, Jr., J. Chem. Phys. **55**, 3236 (1971).
[21] D. A. King, T. E. Madey, and J. T. Yates, Jr., J. Chem. Phys. **55**, 3247 (1971).
[22] P. Alnot, D. J. Auerbach, J. Behm, C. R. Brundle, and A. Viescas, Surf. Sci. **213**, 1 (1989).
[23] E. Bauer, H. Poppa, and Y. Viswanath, Surf. Sci. **58**, 517 (1976).
[24] R. W. G. Wyckoff, *Crystal Structure*, 2nd ed. (Wiley, New York, 1963).
[25] K. Jacobi, E. S. Jensen, T. N. Rhodin, and R. P. Merrill, Surf. Sci. **108**, 397 (1981).
[26] P. A. Thiel and T. E. Madey, Surf. Sci. Rep. **7**, 211 (1987).
[27] F. P. Netzer and T. E. Madey, Surf. Sci. **119**, 422 (1982).
[28] D. L. Doering and T. E. Madey, Surf. Sci. **123**, 305 (1982).
[29] U. Diebold and T. Madey, J. Vac. Sci. Technol A **10**, 2327 (1992).
[30] G. Pirug, C. Ritke, and H. P. Bonzel, Surf. Sci. **241**, 289 (1991).
[31] H. Niehus, W. Heiland, and E. Taglauer, Surf. Sci. Rep. **17**, 213 (1993).
[32] E. L. Román, J. L. de Segovia, R. L. Kurtz, R. Stockbauer, and T. E. Madey, Surf. Sci. **273**, 40 (1992).
[33] D. G. Aitken, P. A. Cox, R. G. Egdell, M. D. Hill, and I. Sach, Vacuum **33**, 756 (1983).
[34] R. L. Kurtz and V. Henrich, Phys. Rev. B **26**, 6682 (1982).
[35] R. L. Kurtz, R. Stockbauer, T. E. Madey, E. Román, and J. L. de Segovia, Surf. Sci. **218**, 178 (1989).
[36] P. Klein, M. Vicanek, and H. Urbassek, Phys. Rev. B **51**, 4597 (1995).
[37] M. V. V. S. Rao and S. K. Srivastava, J. Phys. B **25**, 2175 (1992).
[38] J. Schutten, F. J. D. Heer, H. R. Moustafa, A. J. H. Boerboom, and J. Kistemaker, J. Chem. Phys. **44**, 3924 (1959).
[39] T. D. Mark and F. Egger, Int. J. Mass. Spectrom. Ion. Phys. **20**, 89 (1976).
[40] M. L. Knotek, Surf. Sci. **101**, 334 (1980).
[41] T. E. Madey, D. E. Ramaker, and R. Stockbauer, Annu. Rev. Phys. Chem. **35**, 215 (1984).
[42] P. J. Feibelman and M. L. Knotek, Phys. Rev. B **18**, 6531 (1978).
[43] T. E. Madey, Surf. Sci. **33**, 355 (1972).
[44] S. A. Chambers, Surf. Sci. Rep. **16**, 261 (1992).
[45] E. W. McDaniel, J. B. A. Mitchell, and M. E. Rudd, *Atomic Collisions: Heavy Particle Projectiles* (Wiley–Interscience, New York, 1993).
[46] F. Linder, in *Electronic and Atomic Collisions*, edited by H. B. Gilbody, W. R. Newell, F. H. Read, and A. C. H. Smith (Elsevier, New York, 1988), p. 287.
[47] T. Su and M. T. Bowers, in *Gas Phase Ion Chemistry*, edited by M. E. Bowers (Academic, New York, 1979), p. 83.
[48] O. Dutuit, in *Fundamentals of Gas Phase Ion Chemistry*, edited by K. R. Jennings (Kluwer Academic, Netherlands, 1991), p. 21.
[49] J. A. Olson and B. J. Garrison, Nucl. Instrum. Methods Phys. Res. B **14**, 414 (1986).
[50] B. H. Bransden and M. R. C. McDowell, *Charge Exchange and the Theory of Ion-Atom Collisions* (Clarenden, Oxford, 1992).
[51] R. E. Johnson and J. W. Boring, in *Collision Spectroscopy*, edited by R. G. Cooks (Plenum, New York, 1978), p. 91.
[52] D. Rapp and W. E. Francis, J. Chem. Phys. **37**, 2631 (1962).
[53] I. Dotan and W. Lindinger, J. Chem. Phys. **76**, 4972 (1982).
[54] J. B. Hasted, *Physics of Atomic Collisions*, 2nd ed. (Elsevier, New York, 1972).
[55] D. L. Albritton, At. Data Nucl. Data Tables **22**, 1 (1978).
[56] D. Smith, N. G. Adams, and T. M. Miller, J. Chem. Phys. **69**, 308 (1978).